International Journal of Nanomedicine

Dovepress
open access to scientific and medical research

Open Access Full Text Article

ORIGINAL RESEARCH

Preparation of Ultra-Small Copper Nanoparticles-Loaded Self-Healing Hydrogels with Antibacterial, Inflammation-Suppressing and Angiogenesis-Enhancing Properties for Promoting Diabetic Wound Healing

Xinrong Geng, Kang Liu, Jinlei Wang, Xiangchen Su, Yijie Shi, Liang Zhao

School of Pharmacy, Jinzhou Medical University, Jinzhou, 121000, People's Republic of China

Correspondence: Yijie Shi; Liang Zhao, Tel +86 (0)416 4673430, Fax +86 (0)416 4673439, Email shiyijie119@163.com; liangzhao79@163.com

Background: Bacterial invasion, protracted inflammation, and angiogenesis inhibition are hallmarks of chronic diabetic wounds, bringing about patient morbidity and rising healthcare costs. For such wounds, there are currently few efficient therapies available.

Methods: We reported the development of carboxymethyl chitosan (CMCS)-based self-healing hydrogel loaded with ultra-small copper nanoparticles (Cunps) for local treatment of diabetic wound healing. The structure of Cunps was identified by XRD, TEM, XPS and other methods, and the characterization of the synthesized Cunps-loaded self-healing carboxymethyl chitosan (CMCS)-protocatechualdehyde (PCA) hydrogel (Cunps@CMCS-PCA hydrogel) was further investigated. The therapeutic effect of Cunps@CMCS-PCA hydrogel in diabetic wound healing was explored in vitro and in vivo.

Results: The findings showed that a kind of ultra-small size copper nanoparticles with excellent biocompatibility was prepared. CMCS was chemically conjugated to PCA to form self-healing hydrogels via the formation of an amide bond followed by the loading of ultra-small copper nanoparticles. The obtained Cunps@CMCS-PCA hydrogel showed a typical three-dimensional interlinked network structure with self-healing ability and porosity. It exhibited good biocompatibility in diabetic wounds. Furthermore, Cunps@CMCS-PCA hydrogel group significantly prevented bacterial growth in the skin wound of diabetic rats as compared to model group and CMCS-PCA hydrogel-treated group. After 3 days, no visible bacterial proliferation was observed. It also increased angiogenesis through Cunps mediated activation of ATP7A to prevent induction of autophagy. Furthermore, Cunps@CMCS-PCA hydrogel mainly depended on PCA-induced inhibition on inflammation of macrophage via JAK2/STAT3 signaling pathway. As a result, compared with delayed wound healing process with lower wound healing rate valued at 68.6% within 7 days in the model group, Cunps@CMCS-PCA significantly accelerated wound healing recovery and increased wound healing rate to 86.5%, suggesting that Cunps@CMCS-PCA hydrogel effectively accelerated wound healing.

Conclusion: Cunps@CMCS-PCA hydrogel offered a new therapeutic approach for quickening diabetic wound healing.

Keywords: chronic diabetic wounds, wound healing, copper nanoparticles, carboxymethyl chitosan, protocatechualdehyde, hydrogel

Introduction

The wound healing process is continuous events which can be divided into four separate but overlapping steps; these include hemostasis, inflammation, proliferation and remodeling. In terms of chronic wound healing, it was characterized by severe scarring, inflammation and prolonged healing time.[1] Especially during the occurrence of diabetic wound healing, numerous distinct cell types are regulated at various phases of the biological process.[2] The limitations of diabetic chronic repairment are mainly manifested as reduced neovascularization and collagen deposition, prolonged inflammatory reaction, and enhanced oxidative stress. Although many new treatment methods including autologous skin

Received: 1 December 2022
Accepted: 8 May 2023
Published: 19 June 2023

transplantation, revascularization, negative pressure suction and stem cell therapy show the promising therapeutic potential, high cost of treatment, clinical effectiveness and safety limit their application in medical practice.[3] At the location of the diabetic wound injury, bacteria such *Staphylococcus aureus* and *Escherichia coli* initially multiply, leading to chronic bacterial infections and excessive local inflammation.[4] In addition, activated pro-inflammatory macrophages secrete a greater quantity of pro-inflammatory cytokines, which maintains an excessive level of inflammation at the wound site and slows the progression from the inflammatory phase to the proliferative phase.[5] The diabetic wound injury is also characterized by impaired angiogenesis and poor vascular integrity.[6] Taken together, in order to promote wound healing process, the multifaceted therapy should be made in killing bacteria, increasing angiogenesis, and reducing inflammation.

Neovascularization is significantly aided by the crosstalk between autophagy and copper transporter ATP7A in endothelial cells. Recent studies have demonstrated that excessive autophagy activation and lower expression of copper transporter ATP7A protein can be found in human umbilical vein endothelial cells (HUVECs) cultured under high glucose (HG) conditions as well as in diabetic db/db animals, thus resulting in poor wound healing.[7–9] Furthermore, VEGFR2-mediated angiogenesis are selectively regulated owing to ATP7A's binding to VEGFR2 in endothelial cells (ECs) for preventing VEGFR2 ubiquitination and VEGFR2-targeted lysosomal degradation. The formation of autophagy lysosomes and autophagy flux are promoted by ATP7A deletion, which speeds up the degradation of VEGFR2 protein. Therefore, the down-regulation of ATP7A may lead in the reduction of VEGFR2 expression, which may impair angiogenesis in diabetic peripheral artery disease.[10,11] The up-regulation of ATP7A in diabetic wounds may represent a feasible therapeutic means of enhancing angiogenesis.

Copper (Cu) as an indispensable trace element is reported to take part in the healing process for wounds.[12–14] Particularly, the addition of copper can activate copper transporter ATP7A, which in turn inhibits autophagy and increases the expression of VEGFR2.[15,16] Diabetic wound healing rates are reportedly increased by the delayed release of Cu^{2+} from copper-based metal-organic framework nanoparticles.[17] CuO_2 nanodots that have been sprayed on the wound site have been shown to be effective against MRSA, to reduce inflammation, to encourage angiogenesis, and to speed up the wound healing process.[18] Ultra-small size copper nanoparticles have less long-term toxicity and adverse effects than large-sized Cu nanoparticles due to their ultra-small size and rapid clearance.[19] Some hydrogels containing ultra-small Cu nanoparticles have been developed to control inflammation and promote wound healing.[20] Hydrogel containing ultra-small CuS nanoparticles can effectively increase collagen deposition, up-regulate VEGF expression, and enhance angiogenesis, in which ultra-small copper nanoparticles play a coordinated role in promoting angiogenesis.[21] As a new type of "smart" hydrogels, self-healing polysaccharide-based hydrogels may repair internal damage and recreate 3D polymer networks by dynamic interaction between polymer chains.[22] They are widely employed in wound dressings due to their exceptional qualities including outstanding antibacterial and hemostatic capabilities, mechanical strength, excellent self-healing properties, quick gel performance and good stability.[23,24] In recent years, the research based on carboxymethyl chitosan (CMCS) in the field of medical application has attracted more and more attention. CMCS, as an amphiphilic compound derived from chitosan, shows excellent water solubility, biocompatibility, controllable biodegradability and good antibacterial ability. Furthermore, CMCS has been widely studied and applied in the treatment of chronic skin wound healing.[25] Protocatechualdehyde (PCA), a naturally phenolic molecule from the medicinal plant *Salvia miltiorrhiza*, is reported to not only exhibit its anti-inflammatory properties but also represent a new class of active biomaterial for the production of hydrogels.[26] PCA inhibits the release of inflammatory cytokines from macrophages stimulated by lipopolysaccharide (LPS).[27] Additionally, it has the ability to control the JAK2/STAT3 signaling pathway and prevents the activation of inflammation.[28,29]

In order to overcome several common limitations encountered in conventional treatment of the chronic diabetic wound, we proposed the ultra-small Cu nanoparticles (Cunps)-loaded self-healing CMCS-PCA hydrogel (Cunps@CMCS-PCA hydrogel), as shown in Figure 1. For the creation of sophisticated hydrogel, CMCS was bioconjugated with PCA via covalent amide bonds to form self-healing and anti-bacterial hydrogel. Cunps were prepared and loaded in hydrogel, which enhanced angiogenesis via Cunps induced VEGF secretion and activation of ATP7A for prevention of autophagy. Cunps@CMCS-PCA hydrogel mainly relied on PCA to inhibit the activation of pro-

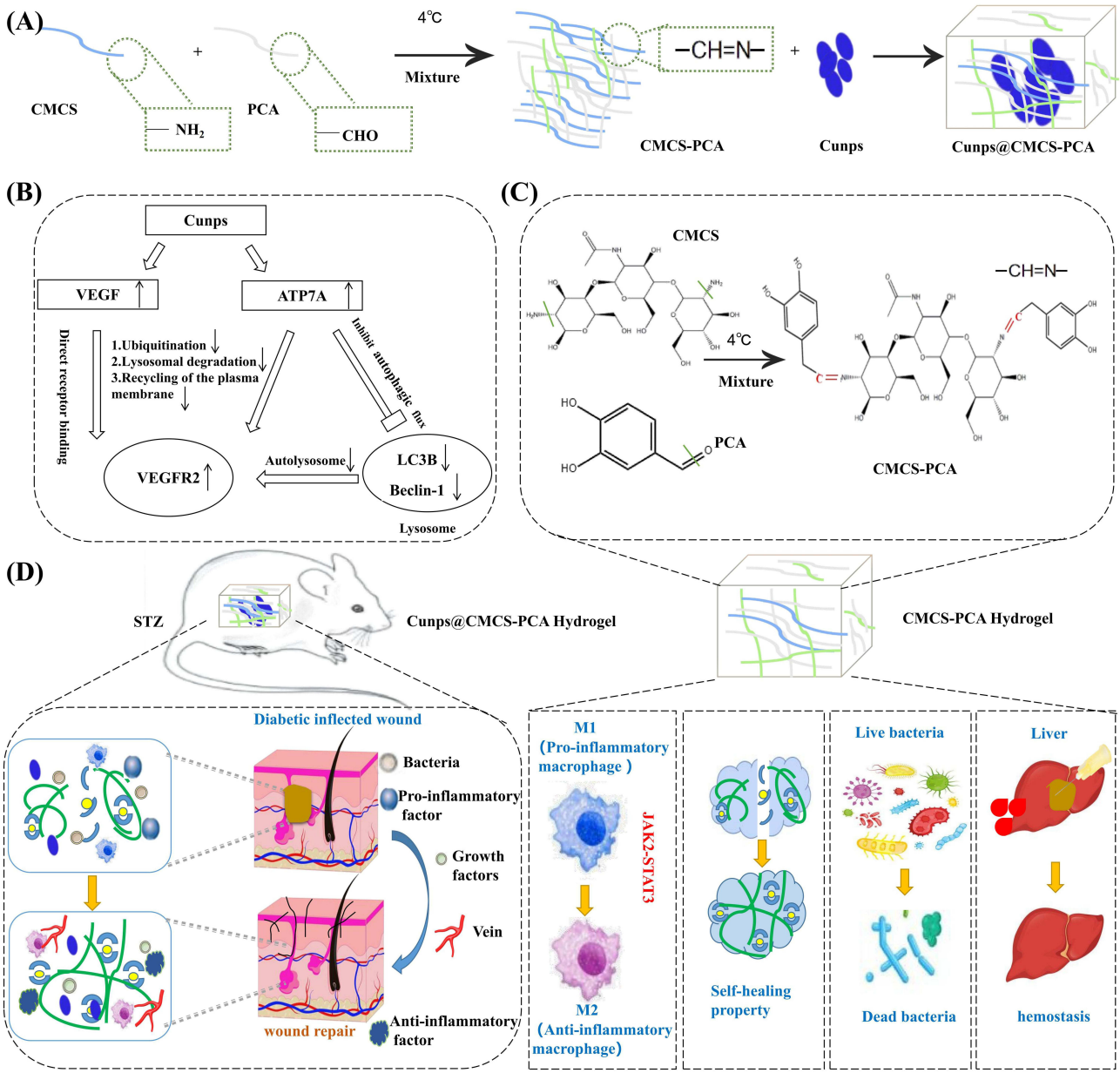

Figure 1 The primary hypothesis of synthesis and potential wound healing applications of Cunps@CMCS-PCA hydrogel. (**A**) Schematic diagram of the formation of Cunps@CMCS-PCA hydrogel. The main components include CMCS, PCA, and Cunps. (**B**) The potential angiogenic mechanisms of Cunps in diabetic wound healing. (**C**) Synthetic process of CMCS-PCA hydrogel. (**D**) Cunps@CMCS-PCA hydrogel improved wound healing in type 1 diabetic rat model.

inflammatory macrophage and attenuate inflammatory response. As a result, it is proposed that the antibacterial Cunps@CMCS-PCA hydrogel could promote diabetic wound healing in diabetic rats.

Materials and Methods

Materials

Carboxymethyl chitosan (degree of substitution ≥90%, isoelectric point: 3–4) was brought from Shanghai McLean Biochemical Technology Co., Ltd. (Shanghai, China); 3,4-dihydroxybenzaldehyde with a molecular weight of 138.12 was obtained from Shanghai McLean Biochemical Technology Co., Ltd. (Shanghai, China). Adenine (purity ≥98%, molecular weight 135.14) was obtained from Beijing Coolebo Technology Co., Ltd. (Beijing, China). Antibodies including LC3B (1:1000, ZEN-BIOSCIENCE, Chengdu, China), Beclin-1, TNF- α, IL-1β (1:1000, WanLeiBio, China, Shenyang), VEGF (1:1000,

WanLeiBio, Shenyang, China), ATP7A (1:1000, Soleibo, Beijing, China), β-actin (1:5000, HUABIO, Jinan, China), JAK2, STAT3, VEGFR2 and CD31 (1:1000, HUABIO, Jinan, China), INOS (1:1000, Affinity Biosciences, USA), CD206 (1:1000, Affinity Biosciences, USA) were obtained. All of the other compounds purchased were of an analytical quality and were sourced from a variety of different vendors. EarthOx Life Sciences in Millbrae, California, USA, provided the goat anti-rabbit IgG/HRP secondary antibody. The American Type Culture Collection supplied the *Staphylococcus aureus* (ATCC 25923) and *Escherichia coli* (ATCC 25922) bacteria strains. The Sprague Dawley rats with the total number of more than 70 that Jinzhou Medical University provided had a body weight ranging from 220 to 250 g each individual. The experimental methodology was approved by the Institutional Animal Care and Use Committee of Jinzhou Medical University, and it was carried out in compliance with the National Guidelines for Animal Protection.

Cells Culture

Human umbilical vein endothelial cells (HUVECs) were obtained from the Cell Bank of the Chinese Academy of Sciences in Shanghai, China. HUVECs were cultured in F12 medium with 10% fetal bovine serum (Gibco BRL). High glucose-cultured HUVECs (HG-HUVECs) were frequently used to simulate the diabetic environment in vitro. These HG-HUVECs were obtained by treating HUVECs with high glucose (HG; 40 mM) for 72 hours (the medium was changed every 24 hours), as was previously described.[30] Murine macrophage RAW264.7 cell line was purchased from American Type Culture Collection (ATCC) and cultured in Dulbecco's Modified Eagle's Medium (DMEM, Hyclone, UT, USA) containing 10% fetal bovine serum (FBS; Gibco, CA, USA) and 1% penicillin–streptomycin (PS). Inflammatory macrophages were stimulated with lipopolysaccharide (LPS, 100 ng/mL) for 24 h.

Synthesis and Characterization of Cunps

After mixing 100 mL of water, 0.34 g of $CuSO_4$, and 0.57 g of adenine, reaction was performed in a water bath at 70 °C under agitation. Finally, the pH was adjusted by adding oxalic acid. After being heated for 5 h, the product was separated from the rest of the system by 30 min of centrifugation at a speed of 15,000 rpm. The resulting Cunps were washed with water, passed through a microporous membrane with a pore size of 0.22 μm, and then dried in a vacuum oven at a temperature of 80 °C for 18 hours. The characterization of Cunps was investigated using X-ray diffraction (XRD) analysis, energy-dispersive X-ray element mapping and spectroscopic analysis (EDS), X-ray photoelectron spectroscopy (XPS), transmission electron microscopy (TEM) and thermogravimetric analysis (TGA). The phase structure and crystallinity of Cunps were identified by X-ray diffraction (XRD, ULTIMAIV RIGAKU, Tokyo, Japan) in the range of 10–80° with a scan rate of 10°/min. The morphology of samples was investigated using transmission electron microscopy (TEM, Tecnai G2 F20, Hillsborough, OR, USA). The valence states of Cu in the samples was characterized by X-ray photoelectron spectroscopy (XPS, PHI QUANTERA-II, ULVAC-PHI, INC., Tokyo, Japan). Thermogravimetric analysis was performed using TA Instrument SDT Q600-0883 (DSC-TGA) equipment with heating rate of 10 °C min^{-1}, flow rate of 100 mL/min, under argon atmosphere, using a crucible of alumina. The MTT assay and the hemolysis test (n=3) were employed, as stated in a study that we had previously published.[31,32] HG-HUVECs and LPS stimulated RAW264.7 cells were incubated with Cunps at different concentrations for 24 hours, respectively. After incubation with serum-free medium containing MTT for 4 hours, DMSO solution was added to each well and the absorbance was measured at 490 nm. Hemolysis test was performed to investigate the biological compatibility of Cunps at varying concentrations. After 15 days of daily intravenous administration of a single dosage of Cunps consisting of 2 mg/kg of body weight, tissue sections from the heart, liver, lung, spleen, and kidney were stained with hematoxylin and eosin (H&E).

Synthesis and Characterization of Cunps@CMCS-PCA Hydrogel

The preparation of Cunps@CMCS-PCA hydrogel was divided into two steps. First, CMCS and PCA solutions were gently stirred (120 rpm) at a volume ratio of 3:1, and then the samples were cooled overnight (4 °C) to create the self-healing CMCS-PCA hydrogel. The prepared Cunps were immersed in CMCS-PCA hydrogel to form Cunps@CMCS-PCA hydrogel. The interaction between PCA and CMCS in the hydrogel was determined by Fourier transform infrared spectroscopy. Briefly, CMCS-PCA hydrogel was ground with KBr powder and pressed into pellets for infrared spectroscopy detection. An investigation into the morphology of Cunps@CMCS-PCA hydrogel was carried out using scanning

electron microscope (**SEM**) (Zeiss SIGMA 500). The samples were cut along the longitudinal direction and cross sections of the slices were sprayed with a thin layer of gold using a sputter coater (Hitachi MC1000). Au was then sprayed on the cross section and the internal structure of the sample was observed using SEM at an accelerating voltage of 5 kV. Using a rotating rheometer, the rheological characteristics of the Cunps@CMCS-PCA hydrogel were evaluated (Anton Paar MCR92). According to the earlier report, the swelling ratio and degrading property of hydrogels were also investigated.[33] Furthermore, the swelling ratio and degradation rate of hydrogels (n=3) were investigated according to the previous report.[34] In order to evaluate the swelling performances of hydrogels, dry hydrogels (W_d) with known weight were immersed in distilled water at room temperature. At different time intervals (t), the swollen gels were taken out from the solution followed by removing excessive water from the surface of the hydrogels, and finally weighed (W_t). The swelling ratio was calculated by the following equation: Swelling ratio (%) = $(W_t - W_d)*100/W_d$. For determining the degradation rate of hydrogels, hydrogels were immersed in 30 mL of PBS (pH 7.4) at a constant temperature (37 °C) and shaken at 100 rpm. At the pre-determined time points, the samples were withdrawn and rinsed with deionized water to remove excessive components, dried for 12 h at 60 °C and then weighed. The mass loss of hydrogels was then defined by the following equation: Mass loss of the hydrogel (%) = $(W_0 - W_t)*100/W_0$, where W_0 and W_t are the dry weights of the hydrogel at the initial and pre-determined time points.

Test on Antibacterial Activities of Cunps@CMCS-PCA Hydrogel

According to the previous report,[35] the antibacterial activity of the hydrogel was measured against *Escherichia coli (E. coli*) and *Staphylococcus aureus* (*S. aureus*) by performing the inhibition zone test. The bacteria were spread evenly over the surface of agar plates by sterile cotton swab. At the same time, the drug-sensitive paper with a diameter of 0.5 cm covered with CMCS solution, CMCS-PCA hydrogel and Cunps@CMCS-PCA hydrogel containing the same concentration of CMCS was then placed on the agar plates. These plates were cultured in an incubator at 37 °C overnight. The antimicrobial performance was assessed by measuring the diameter of antibacterial circle.

The bacterial suspensions containing *E. coli* and *S. aureus* were appropriately diluted so that the bacterial content is about 10^8 CFU/mL. One hundred microliters of each of the bacterial solution and LB medium containing PBS, CMCS-PCA hydrogel and Cunps@CMCS-PCA hydrogel were placed into an EP tube respectively for continuous shaking for 24 h at 37 °C. Finally, the optical density (OD) at a wavelength of 600 nm was measured with a microplate reader (n=3).

Migration Assay

Transwell assays (n=3) and scratch wound tests (n=3) were utilized to determine the migrating ability of HG-HUVECs treated with Cunps, CMCS-PCA hydrogel and Cunps@CMCS-PCA hydrogel, respectively. For the scratch wound experiment, HG-HUVECs were first seeded in a 6-well cell culture plate, and then the cell monolayer was scraped with a 200 μL pipet tip in a line. When Cunps, CMCS-PCA hydrogel and Cunps@CMCS-PCA hydrogel were applied to plates and incubated with cells at 37 °C, HG-HUVECs migration toward the center of the well were observed using the microscope and distance was measured to a precise degree. The migration of HG-HUVECs was detected using the transwell method. HG-HUVECs were pre-seeded in the top layer of a cell culture insert precoated with basement membrane Matrigel. After samples were placed into insert pre-seeded with HG-HUVECs, cells had passed through the membrane and migrated to the lower surface of the filter. The migrated cells may be viewed and counted under an optical microscope (Leica DMI6000B, Germany).

Tube Formation Assay

After HG-HUVECs were resuspended in serum-free medium, cells were deposited into each well of a 24-well plate that had been coated with Matrigel. CMCS-PCA hydrogel and Cunps@CMCS-PCA hydrogel were added to each well for a continuous cell incubation for 8 h. The final step consisted of observing and analyzing HG-HUVECs was performed using an optical microscope (Leica DMI6000B, Germany) and images were captured at a magnification of 100 times. The total branching points and total tube length of HG-HUVECs were determined (n=3).

Establishment of Diabetic Wound Model and Treatment with Formulations

Based on the previous report,[36] to develop Sprague Dawley rats model of type 1 diabetes, the drug streptozotocin (STZ; Sigma-Aldrich Company) was administered by daily intraperitoneal injection to Sprague Dawley rats at a dose of 55 mg/kg/body weight. This was done to ensure that the animals' blood glucose levels were higher than 16.7 mmol/L. Then, rats were anesthetized and hair was then removed, and full thickness resectable skin wounds (diameter: 2 cm) were made on their backs. Finally, 2 weeks of daily application of CMCS-PCA hydrogel and Cunps@CMCS-PCA hydrogel to the wound was completed. Based on the previous report,[37] the reduction in wound size can be determined using the following formula: Wound Healing rate (%) = $(A_0- A_t) \times 100/A_0$, where A_0 is the initial wound area and A_t is the wound area after 3, 7,10, and 14 days of treatment. The assessment of the wound healing process was given by examining images of diabetic wound using a digital camera. In order to conduct an analysis of the pathological changes that took place at the wound site, the surrounding muscles and wound were dissected out and then preserved in 10% formalin. After being dehydrated and then waxed with paraffin, the specimens that were embedded in solid paraffin were cut into a series of slices. Examined wound sections were treated by H&E staining and Masson trichrome staining for visualizing angiogenesis and collagen deposition, and evaluating inflammatory reaction and cell proliferation, which were allowed to determine whether or not the wounds had the potential to heal.[38,39] In addition, immunofluorescence staining was applied to evaluate the inflammatory response by checking the expressions of INOS and CD206 in diabetic wound tissue treated with Cunps@CMCS-PCA hydrogel. The development of blood vessels was also investigated by determining the expression of CD31 in wound site using immunofluorescence and immunohistochemistry methods.

Immunohistochemical Staining

Immunohistochemical staining was performed according to the previous report.[40] After being dewaxed in xylene, the sections went through a rehydration process that used an alcohol gradient. After that, the sections were treated with hydrogen peroxide (H_2O_2) at a concentration of 3% for 10 minutes, and antigen retrieval was accomplished by incubating them at high pressure in citrate buffer for 3 minutes (pH 6.0). After being washed with PBS, the sections were then blocked with goat serum for 20 minutes. The primary antibodies were then incubated at a temperature of 4 °C for a full 24 hours. After this step, the sections were given the incubation with polymer and immunoglobulin (IgG), which was done in accordance with the varied sources of the primary antibodies. After that, the sections that had been stained were seen using a substrate containing 3.3-diaminobenzidine (DAB), and the sections that had been counterstained were stained with hematoxylin. After being cleaned with xylene, the parts were dehydrated with alcohol and then neutral resins were applied to seal them. In order to examine the non-specific staining, certain sections were treated without primary antibodies and instead with normal serum. Under a light microscope and with the assistance of the image analysis software, each segment was scrutinized for its quantitative characteristics.

Immunofluorescence Staining

Following a 24-hour incubation with CMCS, PCA, CMCS-PCA hydrogel, and Cunps@CMCS-PCA hydrogel, the cells were fixed with 4% paraformaldehyde for 30 minutes, permeabilized with 0.1% Triton X-100 for 20 minutes, and then blocked with goat serum for 20 minutes. The cells were then treated with the primary antibodies, and they were kept in an incubator at 4 °C overnight. In the final step, secondary antibodies, such as Texas red-conjugated donkey anti-rabbit IgG or fluorescein isothiocyanate (FITC)-conjugated donkey anti-rat IgG, were added to the cells and allowed to incubate for 1 hour before being removed. An image of fluorescence was seen when viewed via an optical microscope (Leica DMI6000B, Germany).

Western Blot Assay

According to the previous report,[41] proteins are first separated by size or other physical properties by gel electrophoresis. A polyvinylidene fluoride (PVDF) membrane was used to separate protein lysates using 12% SDS-polyacrylamide gel electrophoresis (PAGE) (BioTrace; Pall Corporation, New York, USA). The membrane was incubated with a dilution of the primary antibodies at a concentration of 1:500 overnight at 4 °C after blocking with 1% bovine serum albumin (BSA) at room temperature for 1 hour. Following a wash, a 1:500 dilution of the

secondary antibody was applied to the membrane, which was then incubated for an additional hour at room temperature. After another wash, the membrane was dyed with enhanced chemiluminescence (ECL). With the aid of a UVP gel analysis device, the target protein's level was captured and examined (iBox Scientia 600; UVP, LLC, CA, USA).

Statistical Analysis

The means and standard deviation of all data are presented (SD). ANOVA was used to compare the groups in the one-way fashion. To be statistically significant, a value of *$p < 0.05$, **$p < 0.01$, and ***$p < 0.001$ was used.

Results

Characterization of Cunps

Cunps were found to be spherical in shape and have an average size of just 10 nm according to TEM image (Figure 2A). Cunps' hydrodynamic size was measured using dynamic light scattering (DLS), and the findings demonstrated that the average size of Cunps was approximately 7.1 nm (Figure 2B). The Cunps' X-ray diffraction (XRD) spectra (Figure 2C) showed adenine-specific peaks that corresponded to JCPDS Card no. 04–0567, which was accord with the previous report.[42] Cu may be related with the newly observed diffraction peaks at 2θ=11.69°, 27.34° and 30.72°. The presence of C, N, O, and Cu in Cunps was detected by energy-dispersive X-ray spectroscopy (EDS) (Figure 2D), indicating the effective incorporation of Cu atoms into the adenine. According to elemental mapping and energy-dispersive spectroscopy (EDS) results, Cu elements were uniformly dispersed into Cunps (Figure 2E). The existence of the Cu^{2+} valence state of copper was confirmed by high-resolution XPS spectroscopy (Figure 2F). Being consistent with the previous report,[43] Cu^{2+} was linked to the observable cluster of satellite features at 943.33 eV and 962.68 eV, while the signal at 934.05 eV, attributed to the binding energy of Cu^{2+}, indicated that Cu^{2+} was successfully conjugated to adenine. Figure 2G showed the results of a thermogravimetric analysis (TGA) experiment that was conducted to investigate the thermal stability of Cunps. Prior to 195 °C, the weight loss was frequently caused by a loss of water molecules. Thermal analysis of free adenine had revealed the presence of two decomposition steps, one centered at 383 °C and the second at 667 °C, which were attributed to the loss of $C_4N_3H_3$ and N_2CH_2,[44] while thermal analysis of coordinated adenine had revealed the presence of two degradation steps at similar temperature ranges of 195–408°C and 408–800°C. As a direct consequence of this, compared to free adenine, the proportion of lost mass shifted from smaller values to greater values in the first step, and vice versa in the second step. The binding of N-adenine to copper gave the ring structure its initial degree of rigidity; however, this stiffness began to weaken during the second stage, which coincides with a greater percentage of mass loss. According to MTT studies, Cunps was biocompatible and did not appear to be cytotoxic. The cell survival rate in HG-HUVECs and LPS stimulated RAW264.7 cells in 24 h was still above 80% when the concentration of Cunps was increased to 100 μg/mL (Supplementary Figure 1A). Hemolysis test findings (Supplementary Figure 1C) further demonstrated high blood compatibility of Cunps. In the positive control group that had only pure water treatment, the erythrocytes were fragmented. Contrarily, when treated with Cunps at a concentration of 2 mg/mL, the red blood cells did not suffer hemolysis, indicating that Cunps showed high blood compatibility. By employing H&E staining to examine the histological differences of the main organs, systemic toxicity of Cunps in vivo was assessed. Cunps at 2 mg/kg/body did not cause any evident histological differences in major organs as compared to the sham group (saline treatment), suggesting that Cunps did not cause any substantial toxicity (Supplementary Figure 1B).

Characterization of Cunps@CMCS-PCA Hydrogel

Infrared spectroscopy was used to examine the synthesis and characterization of CMCS-PCA hydrogel. Being consistent with the previous report,[45] in IR spectra of PCA-CMCS hydrogel (Figure 3A), the peak at 1411 cm^{-1} representing CN stretching vibration was observed. In addition, the peak of CMCS-PCA hydrogel at 1587 cm^{-1} was significantly higher than that of pure CMCS and PCA, while the peak at 1635 cm^{-1} was lower, indicating that the amino group of CMCS was covalently connected with the carboxyl group of PCA through the amide bond, leading to the conversion of primary amine to secondary amine. Both CMCS-PCA hydrogel and Cunps@CMCS-PCA hydrogel underwent in vitro swelling

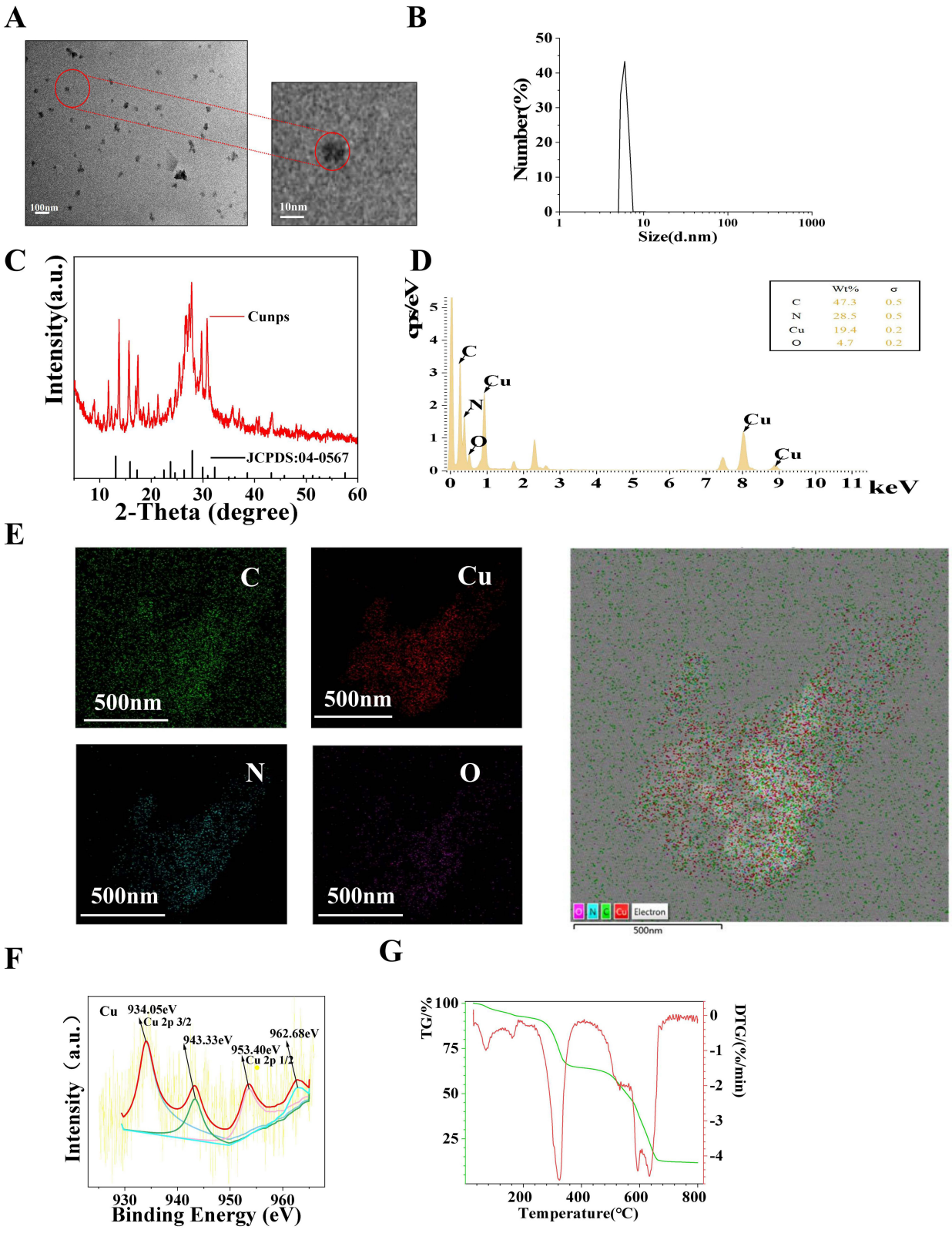

Figure 2 Characterization of Cunps. (**A**) TEM image of Cunps. (**B**) Particle size distribution of Cunps measured by DLS. (**C**) XRD pattern of Cunps. (**D**)The energy-dispersive X-ray spectrum of Cunps. (**E**) Energy-dispersive spectrometer (EDS) mapping images of C, N, Cu and O. (**F**) The expanded regions of XPS spectra showing the peaks of Cu(2p) of Cunps. (**G**) Thermogravimetric analysis (TGA) of Cunps.

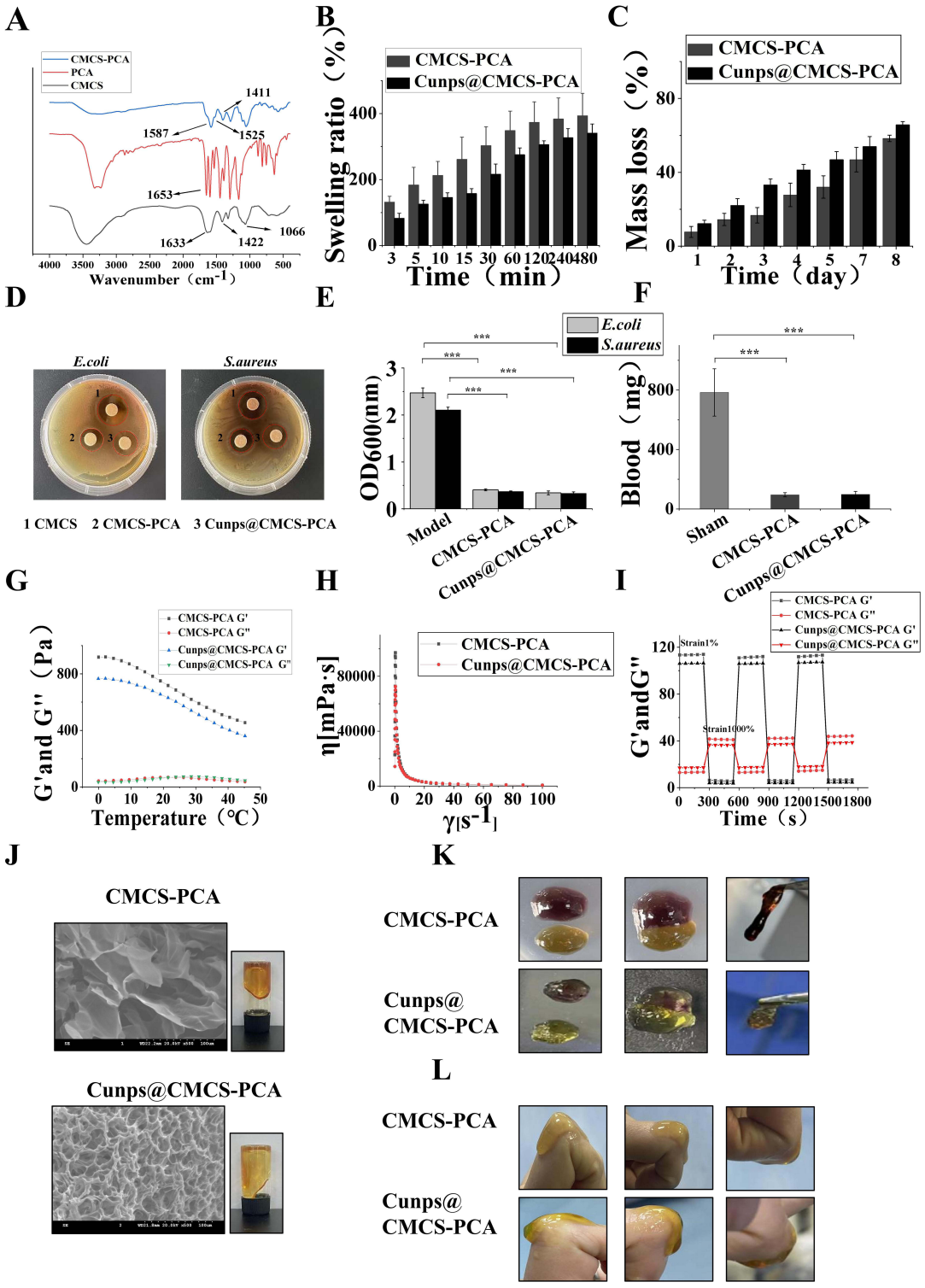

Figure 3 Structure and multifunctional properties of CMCS-PCA hydrogel and Cunps@CMCS-PCA hydrogel. (**A**) FTIR of CMCS, PCA, CMCS-PCA hydrogel. (**B**) Swelling changes of CMCS-PCA hydrogel and Cunps@CMCS-PCA hydrogel at 37 °C, data are mean ± SD (n=3). (**C**) Degradation determination of CMCS-PCA hydrogel and Cunps@CMCS-PCA hydrogel in PBS, data are mean ± SD (n=3). (**D**) Inhibition zone images of CMCS solution, CMCS-PCA hydrogel and Cunps@CMCS-PCA hydrogel. (**E**) Determination of the viability of the bacterial suspension containing CMCS-PCA hydrogel and Cunps@CMCS-PCA hydrogel. The untreated bacterial suspension was set as model group. These data are representative of three independent experiments and are expressed as mean ± SD, ***$p < 0.001$. (**F**) Analysis of hepatic hemorrhage in Sprague Dawley rats treated with CMCS-PCA hydrogel and Cunps@CMCS-PCA hydrogel. The bleeding amount was determined after the application of the hydrogel to the hepatic bleeding site. We took the untreated bleeding site as the sham group. Data are representative of three independent experiments and are presented as mean ± SD, ***$p < 0.001$. (**G**) Storage and loss moduli of CMCS-PCA hydrogel and Cunps@CMCS-PCA hydrogel with changes of temperature. (**H**) Viscosity of CMCS-PCA hydrogel and Cunps@CMCS-PCA hydrogel with changes of shear stress. (**I**) G' and G" of CMCS-PCA hydrogel and Cunps@CMCS-PCA hydrogel when the step strain was switched from 1% to 1000% at 37°C. (**J**) SEM images of CMCS-PCA hydrogel and Cunps@CMCS-PCA hydrogel at room temperature. (**K**) Photographs of the self-healing adhesive behavior of CMCS-PCA hydrogel and Cunps@CMCS-PCA hydrogel. (**L**) Images of CMCS-PCA hydrogel and Cunps@CMCS-PCA hydrogel with joint bending.

and degradation assays. As seen in Figure 3B and C, it was discovered that as the swelling capacity of both CMCS-PCA hydrogel and Cunps@CMCS-PCA hydrogel increased over time, more water was absorbed, and high swelling ratios of 373% for CMCS-PCA hydrogel and 306% for Cunps@CMCS-PCA hydrogel within 120 min were obtained. Furthermore, the prolonged degradation of both hydrogels depended on the passage of time, showing that the hydrogel network had slowly collapsed, which caused the component's release.

We further investigated antibacterial activities of both hydrogels against gram-positive and gram-negative bacteria. It was established in Figure 3D and 3E that owing to the antibacterial activities of CMCS, CMCS-PCA hydrogel and Cunps@CMCS-PCA hydrogel considerably reduced the growth of *S. aureus* and *E. coli*, as evidenced by larger diameter of the bacterial inhibition zone. Furthermore, we also evaluated the haemostatic properties of hydrogels using a rat model of massive hepatic haemorrhage by determining the amount of bleeding after applying the hydrogels in the bleeding site of liver and comparing the results with the untreated wounds. It was discovered that Cunps@CMCS-PCA hydrogel exhibited good hemostatic capabilities, and the total blood loss in the Cunps@CMCS-PCA hydrogel group was significantly lower than that in the untreated wounds as sham group (98.5±20.2 mg vs 783.8±159.6 mg) (Figure 3F). The rheological properties of hydrogels can be achieved by measuring the energy storage modulus (G') and the energy loss modulus (G") over a specific temperature range. Figure 3G showed thermal scanning rheological studies of the Cunps@CMCS-PCA hydrogel's elastic and viscous modulus. It was clear that with the increase in temperature, the energy storage modulus (G') of CMCS-PCA hydrogel and Cunps@CMCS-PCA hydrogel decreased, while the energy loss modulus (G") maintained a certain constant range. Furthermore, both hydrogels were in a colloidal state owing to the fact that the energy storage modulus (G') in CMCS-PCA hydrogel and Cunps@CMCS-PCA hydrogel was bigger than the energy loss modulus (G"). The flow curves that were estimated at a variety of shear rates and temperatures were presented in Figure 3H. When the shear rate was increased, there was an immediate reduction in the gels' viscosities. As the shear rate continued to progressively increase, the gel's viscosity slowly declined and tended to be slightly changed, demonstrating behavior consistent with shear thinning. As can be seen in Figure 3I, each hydrogel's G' reduced from approximately ~100 Pa to a few Pa when the step strain was increased from 1% to 1000%. Due to the high dynamic strain (1000%) that caused the hydrogel network to collapse after two cycles of stepped strain, the G' value was reduced. However, after reducing the dynamic strain to 1%, the Cunps@CMCS-PCA hydrogel quickly returned to its original G' value, indicating that the hydrogel quickly regained its original structure and good self-healing properties.

Cunps@CMCS-PCA hydrogel and CMCS-PCA hydrogel's porous structure were both visible in SEM images (Figure 3J). The hydrogel's gel structure was not changed during the incorporation of Cunps, and pore size in Cunps@CMCS-PCA hydrogel tended to be smaller as compared to CMCS-PCA hydrogel. The hydrogel's strong covalent connections can spontaneously rebuild and recrosslink when the colloidal structure is artificially damaged, as shown by the self-healing images of the CMCS-PCA hydrogel and Cunps@CMCS-PCA hydrogel (Figure 3K). When CMCS-PCA hydrogel and Cunps@CMCS-PCA hydrogel were applied to the skin, neither hydrogel was easily removed from the skin with joint rotation, further demonstrating the dressing's viscosity (Figure 3L).

Cunps@CMCS-PCA Hydrogel Enhanced Angiogenesis via Cunps Stimulated VEGF Secretion and Activation of ATP7A to Prevent Induction of Autophagy

As angiogenesis is a crucial step in the repairment of skin wounds and helps generate and remodel new blood vessels,[46] we first investigated whether Cunps can induce the angiogenesis response of HG-HUVECs. Figure 4A and B showed that the migration rate was significantly increased after HG-HUVECs were incubated with Cunps for 12 and 24 hours, and Figure 4C and D showed that Cunps induced the higher number of migrated HG-HUVECs as compared to untreated HG-HUVECs, indicating the ability of Cunps to promote migration of HG-HUVECs in vitro. Cunps@CMCS-PCA hydrogel, in particular, induced the highest migration rate in HG-HUVECs and the maximum number of cells to penetrate through the chamber. Results from Matrigel tube formation (Figure 4E and 4F) further demonstrated that Cunps promoted tube formation by increasing the linked cell and tube counts in arbitrarily chosen locations as compared to the untreated HG-HUVECs group. In particular, when compared to the other treatment groups, the number of vascular loops and branches

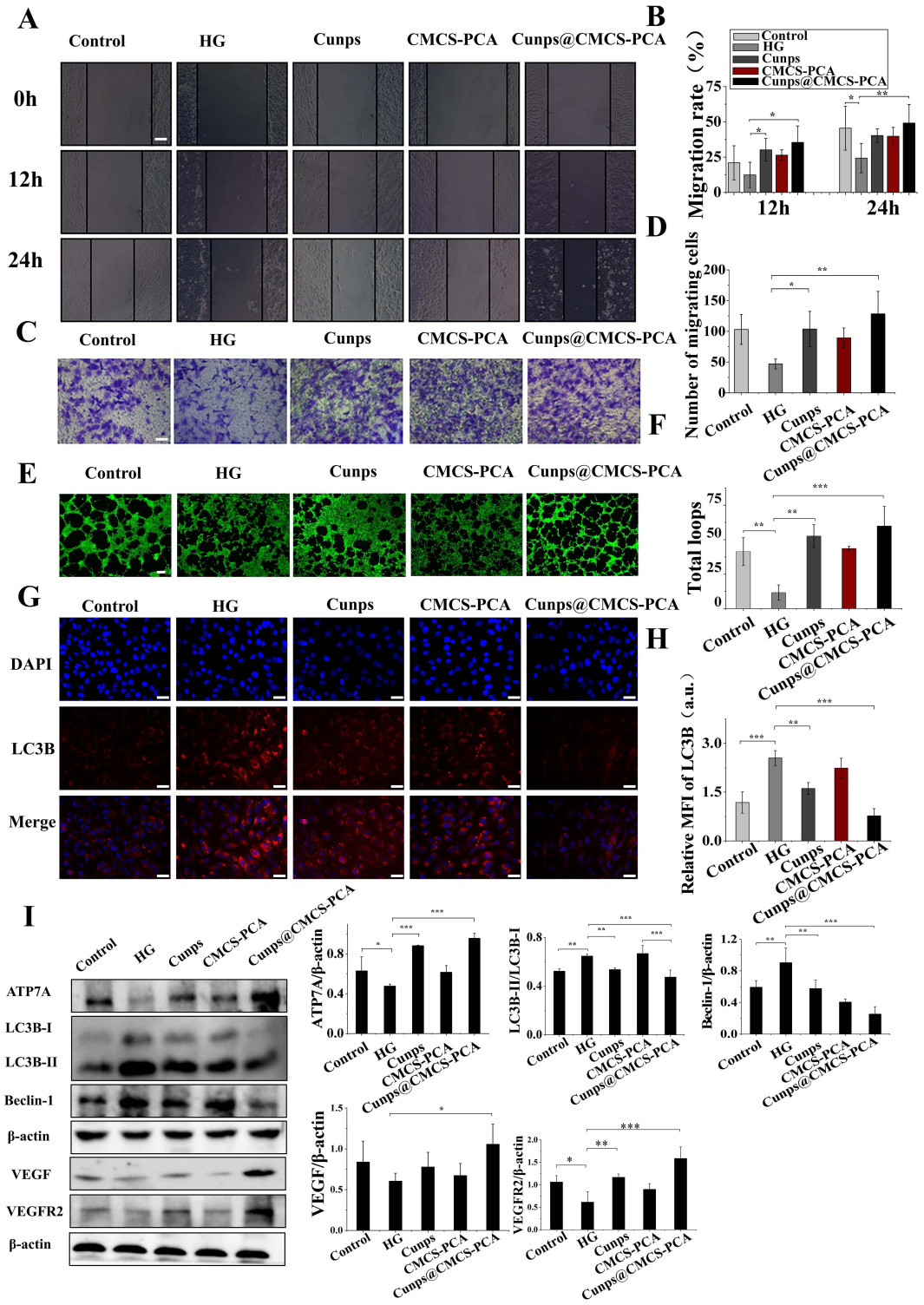

Figure 4 Cunps@CMCS-PCA hydrogel induced angiogenesis in vitro. Normal HUVECs were set as control group. (**A**) Cell scratch assay in in HG-HUVECs treated with Cunps, CMCS-PCA hydrogel, and Cunps@CMCS-PCA hydrogel at 12 and 24 hours following a single scratch. Images were taken at 12 and 24 hours after the scratch. The scale bar is set at 100 μm. (**B**) Determination on cell migration rate in different groups. *$p < 0.05$, **$p < 0.01$; data reflect mean ± SD (n=3). (**C**) Migration pictures of HG-HUVECs treated with Cunps, CMCS-PCA hydrogel, and Cunps@CMCS-PCA hydrogel. A scale bar of 100 μm is used. (**D**) A quantitative examination of the number of migrated cells in different groups. *$p < 0.05$, **$p < 0.01$; data reflect mean ± SD (n=3). (**E**) In vitro tube formation assay in HG-HUVECs following Cunps, CMCS-PCA hydrogel, and Cunps@CMCS-PCA hydrogel treatments. A scale bar of 100 μm is used. (**F**) Total loops were measured. Data represent mean ± SD (n=3), **$p < 0.01$, ***$p < 0.001$. (**G**) Immunofluorescence detection of LC3B in HG-HUVECs treated with Cunps, CMCS-PCA hydrogel, and Cunps@CMCS-PCA hydrogel. The 100 μm scale bar is used. (**H**) Intracellular LC3B immunoquantification (red). Data are expressed as mean ± SD (n=3), **$p < 0.01$, ***$p < 0.001$. (**I**) Western blot images and analysis of ATP7A, VEGF, VEGFR2, Beclin-1, LC3B-II/LC3B-I after 24 h of HG-HUVECs treated with Cunps, CMCS-PCA hydrogel and Cunps@CMCS-PCA hydrogel. Data represent mean ± SD (n=3), *$p < 0.05$, **$p < 0.01$, ***$p < 0.001$.

was higher in the group treated with Cunps@CMCS-PCA hydrogel. All of these observations pointed to the possibility that Cunps@CMCS-PCA hydrogel promoted HG-HUVECs angiogenesis in vitro.

Endothelial autophagy has been demonstrated to be activated in diabetic wound sites than in normal skin, which exhibited a negative impact on diabetic wound tissue healing by limiting angiogenesis.[47] The expression of VEGFR2 can increase as a result of inhibition of copper transporter ATP7A mediated autophagy via the addition of copper. We therefore explored whether Cunps controlled angiogenesis was mediated by the regulation of copper transporter ATP7A and autophagy. According to Figure 4G-I, compared with normal HUVECs, immunofluorescence results showed that expression of LC3B protein in HG-HUVECs was dramatically elevated and western blot results also confirmed that the levels of the autophagy-related proteins LC3B II/LC3B I and Beclin-1 were much higher, while the expression of ATP7A and VEGFR2 was lower, indicating that HG down-regulated ATP7A and induced autophagy for accelerating the degradation of VEGFR2. On the contrary, the addition of Cunps promoted the entry of copper transporter ATP7A into cells as evidenced by the higher expression of ATP7A, and further prevented autophagy by reducing fluorescence intensity of LC3B protein and decreasing levels of LC3B II/LC3B I and Beclin-1. As a result, the expression of VEGFR2 was increased owing to the prevention of degradation of VEGFR2 in autolysosome. Meanwhile, the addition of Cunps also stimulated VEGF secretion. Taken together, it was proven that Cunps in CMCS-PCA hydrogel not only stimulated VEGF secretion but also activated ATP7A to prevent induction of autophagy, thus promoting angiogenesis in vitro.

Cunps@CMCS-PCA Hydrogel Mainly Depended on PCA Mediated Inhibition of Activation of Pro-Inflammatory Macrophage to Attenuate Inflammatory Response in vitro

As diabetic wounds are typically characterized by chronic inflammation and exhibit persistent pro-inflammatory macrophage polarization, it is especially crucial to suppress the inflammatory response and promote a transition of macrophage from pro-inflammatory type to anti-inflammatory phenotype in wound site. According to earlier publications,[48] LPS at 100 ng/mL was added into macrophages for 24 hours in order to replicate the status of macrophages in diabetic wounds. As shown in Figure 5A and C, when compared to the normal macrophages (control group), the expression of INOS was increased and the ratio of CD206 to INOS were significantly decreased in the LPS-stimulated macrophage group, indicating that macrophages were activated to an inflammatory type under the stimulation of LPS. Contrarily, the addition of PCA from PCA, CMCS-PCA hydrogel, and Cunps@CMCS-PCA hydrogel reduced activation of pro-inflammatory macrophage by downregulating INOS expression and enhancing the ratio of CO206 to INOS. Interestingly, CMCS also made a limited contribution on reducing INOS expression and increasing ratio of CD206 to INOS as compared to PCA. Particularly, Cunps@CMCS-PCA hydrogel revealed the lowest levels of INOS in the western blot assay and immunofluorescence assay, proving that Cunps@CMCS-PCA hydrogel mainly depended on PCA to prevent inflammatory polarization of macrophage. Additionally, Cunps@CMCS-PCA hydrogel enhanced anti-inflammatory abilities of macrophages by demonstrating increased CD206 expression and ratio of CD206 to INOS. Western blotting analysis (Figure 5C) showed that Cunps@CMCS-PCA hydrogel induced the lowest levels of TNF-α in LPS-stimulated macrophage, indicating that Cunps@CMCS-PCA hydrogel inhibited the inflammatory response of macrophage. We next studied the role of JAK2/STAT3 signaling pathway on regulating macrophage polarization in vitro. Western blot results showed that LPS stimulated macrophage produced a strikingly higher level of JAK2 and STAT3 with significant differences from normal macrophage. On the contrary, increased expressions of JAK2 and STAT3 in macrophages polarized by LPS were partly abrogated by the addition of PCA, CMCS, CMCS-PCA hydrogel and Cunps@CMCS-PCA hydrogel. Thus, it was concluded that Cunps@CMCS-PCA hydrogel exerted an anti-inflammatory effect in LPS-stimulated macrophages in vitro by promoting the polarization of macrophages from pro-inflammatory state to anti-inflammatory state via inhibited activation of the JAK2/STAT3 signaling pathway.

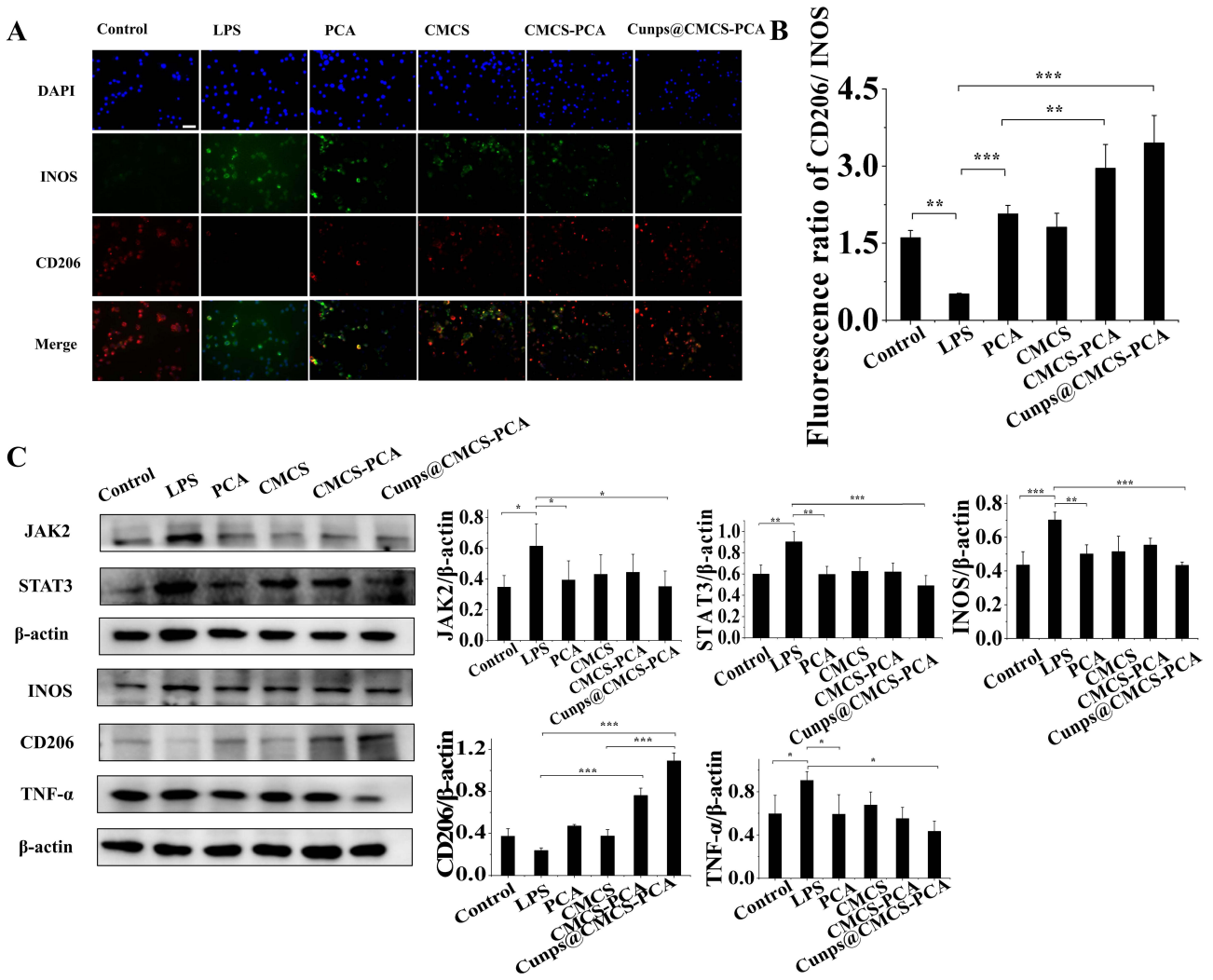

Figure 5 Cunps@CMCS-PCA hydrogel inhibited inflammatory response in LPS-stimulated macrophages by shifting the inflammatory phenotype to the anti-inflammatory phenotype. (**A**) Immunofluorescence images of INOS and CD206 in LPS-stimulated macrophages (RAW264.7) treated with PCA, CMCS, CMCS-PCA hydrogel and Cunps@CMCS-PCA hydrogel for 24 hours. DAPI (blue) as a nuclear marker. The scale bar is set at 200 μm. (**B**) Determination on ratio of CD206 to INOS based on relative fluorescence quantitative analysis; data are mean ± SD (n=3), $^{**}p < 0.01$, $^{***}p < 0.001$. (**C**) Western blot analysis of the expression levels of JAK2, STAT3, INOS, CD206, and TNF-α in LPS-stimulated RAW264.7 macrophages treated with PCA, CMCS, CMCS-PCA hydrogel and Cunps@CMCS-PCA hydrogel for 24 hours. Data represent mean ± SD (n=3), $^{*}p < 0.05$, $^{**}p < 0.01$, $^{***}p < 0.001$.

Cunps@CMCS-PCA Hydrogel Accelerated Diabetic Wound Healing Recovery in Type 1 Diabetic Rats

After validating its potential function on antibacterial ability, boosting angiogenesis, and decreasing inflammatory response in vitro, we explored the promising contribution of Cunps@CMCS-PCA hydrogel on speeding up wound closure and improving wound healing quality in vivo. Type 1 diabetic Sprague Dawley rats (model rats) and normal Sprague Dawley rats with skin wound were then divided into four treatment groups: normal rats treated with PBS (sham group), model rats treated with PBS (model group), CMCS-PCA hydrogel and Cunps@CMCS-PCA hydrogel. According to Figure 6B, CMCS-PCA hydrogel and Cunps@CMCS-PCA hydrogel were found to have high antibacterial activity against both Gram-positive and Gram-negative bacteria at the diabetic wound site when compared to the PBS-treated model group. This was demonstrated by their ability to effectively inhibit bacterial proliferation in the diabetic wound at various time intervals. In particular, Cunps@CMCS-PCA hydrogel significantly prevented bacterial growth in the wound of diabetic rats as compared to the CMCS-PCA hydrogel-treated group. After 3 days, no visible bacterial proliferation was observed. It was claimed that the addition of Cunps as an extra antibacterial agent showed extended and improved

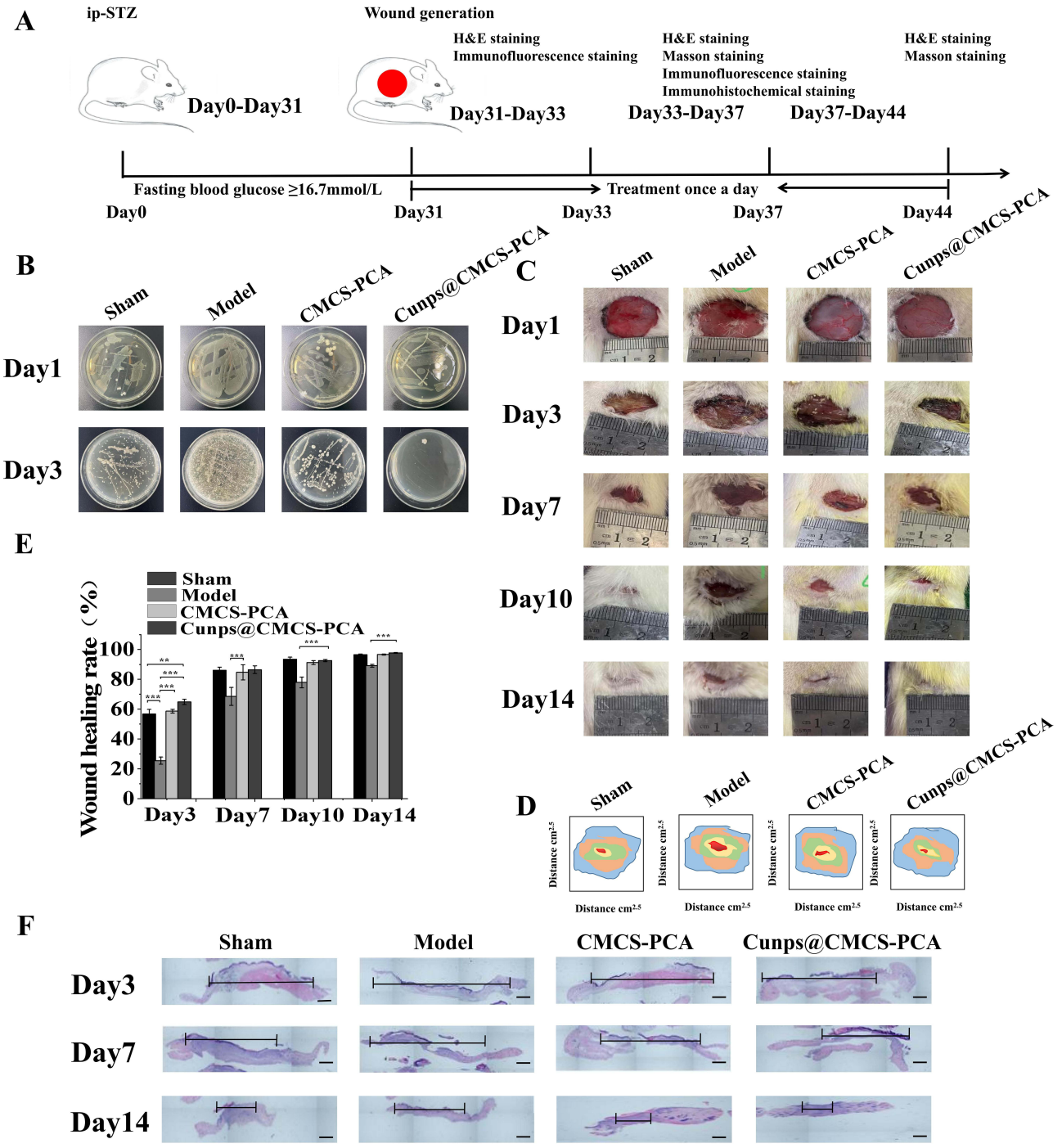

Figure 6 Cunps@CMCS-PCA hydrogel accelerated wound healing process in type 1 diabetic rats. Normal Sprague Dawley rats were used to create the sham-operated group's wounds treated with PBS. The model group consisted of wound in Sprague Dawley rats with type 1 diabetes treated with PBS. (**A**) Schematic diagram of animal experimental design. (**B**) Photos of bacteria in wound exudates from diabetic wound tissues at 1 and 3 days after being administrated with CMCS-PCA hydrogel and Cunps@CMCS-PCA hydrogel. (**C**) Representative images of full-thickness skin defects in type 1 diabetic rats at 1, 3, 7, 10 and 14 days after being administrated with CMCS-PCA hydrogel and Cunps@CMCS-PCA hydrogel. (**D**) Traces of wound closure within 14 days in different groups. (**E**) Determination on wound healing rate of full-thickness skin defect in a type 1 diabetic rat model at 3, 7, 10 and 14 days after being administrated with CMCS-PCA hydrogel and Cunps@CMCS-PCA hydrogel. Data represent mean ± SD (n=3), $^{**}p < 0.01$, $^{***}p < 0.001$. (**F**) Representative H&E staining images of diabetic wound at 3, 7 and 14 days after being administrated with CMCS-PCA hydrogel and Cunps@CMCS-PCA hydrogel. The black scale represents the wound length. The scale bar is set at 2mm.

antimicrobial activity in vivo. Additionally, based on an image of H&E staining, the reepithelialization of the wound area was assessed, and the length of the wound area in diabetic wounds was determined. It was found that CMCS-PCA hydrogel and Cunps@CMCS-PCA hydrogel demonstrated higher level of reepithelialization as compared to the model group, according to Figure 6C-F. The wound area and length in diabetic rats treated with CMCS-PCA hydrogel and Cunps@CMCS-PCA hydrogel were greatly reduced, demonstrating that CMCS-PCA hydrogel and Cunps@CMCS-PCA hydrogel effectively accelerated wound healing.

Cunps@CMCS-PCA Hydrogel Improved the Healing Quality of Diabetic Wound by Inhibiting Inflammation and Enhancing Angiogenesis in vivo

In order to demonstrate whether Cunps@CMCS-PCA hydrogel was beneficial at all stages of chronic diabetic wound healing, we focused on the processes of 3-day inflammatory modulation, 7-day mature vasculation, 14-day granulation and collagen deposition in the diabetic wound site. As seen in Figure 7A, it was found that in terms of the model group, there was a high infiltration of inflammatory cells in diabetic wound tissue. No visible vascular vessels were formed at day 7, while no obvious collagen formation was observed at day 14. By contrast, the wound healing process was obviously accelerated by CMCS-PCA hydrogel and Cunps@CMCS-PCA hydrogel. At day 3, the number of inflammatory cells was lower following treatment with both hydrogels. At day 7, more new blood vessels and a little amount of collagen were observable. Additionally, as compared to CMCS-PCA hydrogel, Cunps@CMCS-PCA hydrogel improved the quality of diabetic wound healing by promoting the development of muscle fibers, hair follicles, and sweat glands. After 14 days, thick collagen with a well-organized collagen fiber structure was also found. In order to evaluate the effectiveness of wound healing, Masson trichrome staining was performed. According to Figure 7E, as compared to the model group and CMCS-PCA hydrogel-treated group, the higher levels of collagen fibers and collagen deposition were observed in Cunps@CMCS-PCA hydrogel-reated group. All these results confirmed that although CMCS-PCA hydrogel and Cunps@CMCS-PCA hydrogel demonstrated the similar wound healing rate with 14 days after administration (Figure 6C-F), Cunps@CMCS-PCA hydrogel significantly improved the wound healing quality by inducing thick collagen deposition and promoting the formation of hair follicles, collagen fibers as compared to CMCS-PCA hydrogel.

We later examined Cunps@CMCS-PCA hydrogel-mediated angiogenesis and inflammation response in the wound. According to the results of immunofluorescence staining and immunohistochemistry, it was found that Cunps@CMCS-PCA hydrogel displayed increased levels of CD31 expression as the characteristic hallmark of endothelial cell vascular proliferation (Figure 7F and G). On the seventh day, the number of new blood vessels was considerably higher in the Cunps@CMCS-PCA hydrogel-reated group than those in the model group and CMCS-PCA hydrogel-treated group. Using immunofluorescence staining and western blotting, we further investigated Cunps@CMCS-PCA hydrogel mediated inflammatory prohibition in diabetic wound site. According to Figure 7C and D, the level of INOS expression elevated and the level of CD206 expression declined in diabetic wound, indicating that the bulk of the macrophages in wound site were inflammatory type. In response to treatment with Cunps@CMCS-PCA hydrogel, the expression of CD206 was elevated, whereas INOS protein expression was downregulated. The strongest red fluorescence, which represented CD206, and the lowest green fluorescence, which represented INOS, were found in Cunps@CMCS-PCA hydrogel-treated group. It indicated that Cunps@CMCS-PCA hydrogel encouraged the conversion of macrophages from the inflammatory type to the anti-inflammatory type. We further explored the reduction of the inflammatory response in view of the role that Cunps@CMCS-PCA hydrogel may promote macrophage polarity from inflammatory type to the anti-flammatory type. Higher levels of IL-6 and IL-1β in diabetic wound tissue showed that the inflammatory response was greatly exacerbated (Figure 7B and D). Cunps@CMCS-PCA hydrogel lowered the levels of IL-6 and IL-1β to reduce the inflammatory response in diabetic wound site. All these results showed that Cunps@CMCS-PCA hydrogel strongly inhibited inflammation by promoting the macrophage functional polarity towards an anti-inflammatory phenotype in vivo.

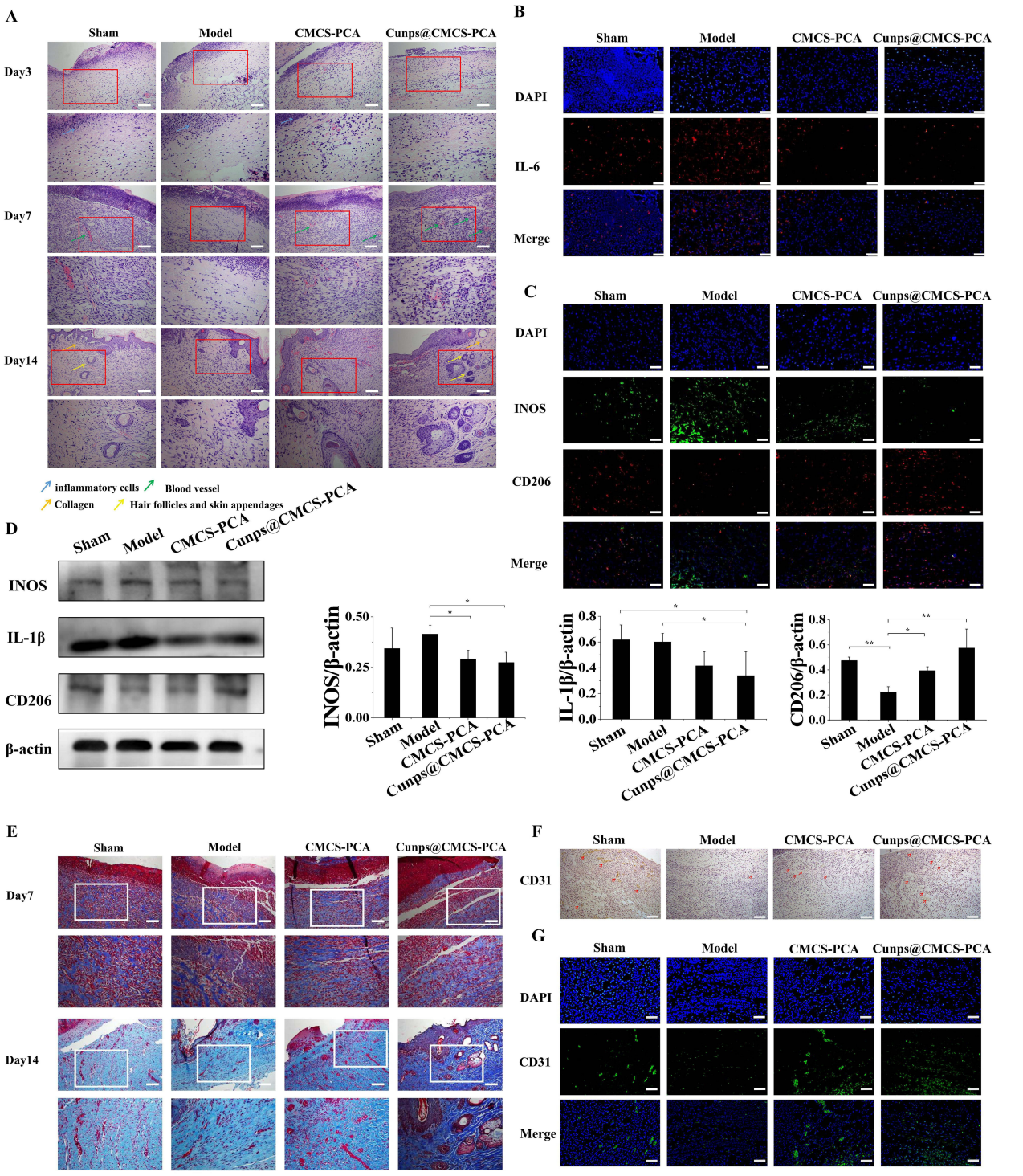

Figure 7 Cunps@CMCS-PCA hydrogel promoted angiogenesis and inhibited inflammation for improving diabetic wound healing quality in vivo. (**A**) H&E staining images of diabetic wounds treated with CMCS-PCA hydrogel and Cunps@CMCS-PCA hydrogel on at day 3, 7 and 14 after administration. The scale bar is 100 μm. (**B**) Immunofluorescence staining images of IL-6 in diabetic wounds treated with CMCS-PCA hydrogel and Cunps@CMCS-PCA hydrogel at day 3 after administration. The scale bar is 100 μm. (**C**) Immunofluorescence staining images of INOS and CD206 expression in diabetic wound tissue treated with CMCS-PCA hydrogel and Cunps@CMCS-PCA hydrogel at day 3 after administration. INOS (green), CD206 (red) and DAPI (blue). The scale bar is 100 μm. (**D**) Western blot analysis on expression levels of INOS, CD206, and IL-1β in diabetic wound tissue treated with CMCS-PCA hydrogel and Cunps@CMCS-PCA hydrogel at day 3 after administration. Data represent mean ± SD (n=3), $*p < 0.05$, $**p < 0.01$. (**E**) Masson's trichrome staining of CMCS-PCA hydrogel and Cunps@CMCS-PCA hydrogel-treated wound sections at day 7 and 14 after administration. The scale bar is 100 μm. (**F**) Immunohistochemical staining images of CD31 in diabetic wounds treated with CMCS-PCA hydrogel and Cunps@CMCS-PCA hydrogel at day 7 after administration. The scale bar is 100 μm. (**G**) Immunofluorescence staining images of CD31 in diabetic wounds treated with CMCS-PCA hydrogel and Cunps@CMCS-PCA hydrogel at day 7 after administration. Vascular endothelial cells (CD31) and nuclei were stained in green and blue. The scale bar is 100 μm.

Discussion

Angiogenesis, the formation of blood vessels, occurs during wound healing. It is an essential step to provide cells with nutrition and oxygen during cutaneous wound healing. Due to metabolic abnormalities, the high glucose environment impaired endothelial cell dysfunction and weakened angiogenesis ability, resulting in the wound healing difficulty.[49] The biological process of chronic wound healing is intricately regulated and involves interactions between several cell types and mediators.[50] The change of ATP7A in type 1 diabetes plays a significant role in neovascularization by affecting VEGFR2-mediated signaling and angiogenesis.[51] This is due to the possibility that VEGFR2 ubiquitination and VEGFR2-targeted lysosomal degradation are prevented by the binding of ATP7A to VEGFR2. Secondly, ATP7A depletion enhanced autophagic flux, including the formation of autophagolysosomes, which hastens the degradation of VEGFR2 protein.

Cu-based nanoparticles have been reported to treat diabetes skin wound healing.[14] Cu is the primary element controlling VEGF expression, promoting endothelial cell growth and migration, and taking part in angiogenesis. It was found that when Cunps we prepared were administered, Cunps stimulated the secretion of VEGF. In the meanwhile, Cunps promoted copper transporter ATP7A entry into cells as shown by the increased expression of ATP7A and further prevented autophagy-mediated degradation of VEGFR2, thus resulting in promotion of angiogenesis.

Because of its high biocompatibility and innate antibacterial activity,[52] polysaccharide-based biomaterials such as CMCS have received a lot of attention. The primary chain of CMCS has a lot of amino groups which can be easily modified by a mild crosslinking reaction.[53] PCA can combine with water-soluble CMCS to form a self-healing hydrogel that can preserve the shape and mechanical strength necessary for treating wound. When the diabetic wound was covered with Cunps@CMCS-PCA hydrogel, it promoted diabetic wound closure by suppressing chronic inflammation, encouraging the creation of granulation tissue, collagen deposition and stimulating neovascularization.

Although Cunps@CMCS-PCA hydrogel has been discussed in the treatment of diabetic wounds and created ultrasmall copper nanoparticles are highly biologically safe based on the time coverage and dose administration, long-term biological safety of Cunps cannot be ignored and should be deeply explored. At the same time, there was an uncertainty about the mechanism of Cunps@CMCS-PCA hydrogel in the treatment of chronic diabetic wounds including how Cunps@CMCS-PCA hydrogel affected other cells and whether Cunps@CMCS-PCA induced diabetic wound healing through other pathways. These problems need to be further clarified and solved.

Conclusion

We created a self-healing hydrogel composed of CMCS and PCA that was loaded with ultra-small copper nanoparticles, and recognized its beneficial impact in expediting diabetic wound healing. The results demonstrated that Cunps@CMCS-PCA hydrogel exhibited antibacterial properties and depended on Cunps mediated activation of ATP7A to stimulate angiogenesis by preventing the autophagic degradation of VEGFR2. PCA as a component of self-healing hydrogels played a major role in inducing the anti-inflammatory transition of macrophage by deactivating the JAK2/STAT3 signaling pathway. Finally, in streptozotocin-induced type 1 diabetic rat models, Cunps@CMCS-PCA hydrogel enhanced wound closure rate and improved the wound healing quality by preventing the proliferation of bacteria, inhibiting inflammation and enhancing angiogenesis in vivo.

Data Sharing Statement

All data generated or analyzed during this study are included in this published article.

Ethical Approval, Consent to Participate and Publication

Research experiments conducted in this article with animals were approved by the Ethical Committee and responsible authorities of Jinzhou Medical University following all guidelines, regulations, legal, and ethical standards as required for animals and followed the National Guidelines for Animal Protection.

Acknowledgments

This work was supported by 2021 Youth Science and Technology Talents Support Plan from Boze Project of Jinzhou Medical University (JYBZQT2105). We thank the support of above funding.

Author Contributions

All authors made a significant contribution to all aspects of this work including the conception, study design, execution, acquisition of data, analysis and interpretation; took part in drafting, revising or critically reviewing the article; gave final approval of the version to be published; have agreed on the journal to which the article has been submitted; and agree to be accountable for all aspects of the work.

Disclosure

The authors report no conflicts of interest in this work.

References

1. Nosrati H, Khodaei M, Alizadeh Z, Banitalebi-Dehkordi M. Cationic, anionic and neutral polysaccharides for skin tissue engineering and wound healing applications. *Int J Biol Macromol*. 2021;192:298–322. doi:10.1016/j.ijbiomac.2021.10.013
2. Ruthenborg RJ, Ban JJ, Wazir A, Takeda N, Kim JW. Regulation of wound healing and fibrosis by hypoxia and hypoxia-inducible factor-1. *Mol Cells*. 2014;37(9):637–643. doi:10.14348/molcells.2014.0150
3. Dixon D, Edmonds M. Managing diabetic foot ulcers: pharmacotherapy for wound healing. *Drugs*. 2021;81(1):29–56. doi:10.1007/s40265-020-01415-8
4. Chumpolphant S, Suwatronnakorn M, Issaravanich S, Tencomnao T, Prasansuklab A. Polyherbal formulation exerts wound healing, anti-inflammatory, angiogenic and antimicrobial properties: potential role in the treatment of diabetic foot ulcers. *Saudi J Biol Sci*. 2022;29(7):103330. doi:10.1016/j.sjbs.2022.103330
5. Song N, Pan K, Chen L, Jin K. Platelet derived vesicles enhance the TGF-beta signaling pathway of M1 macrophage. *Front Endocrinol (Lausanne)*. 2022;18(13):868893. doi:10.3389/fendo.2022.868893
6. Gonzalez AC, Costa TF, Andrade ZA, Medrado AR. Wound healing - a literature review. *An Bras Dermatol*. 2016;91(5):614–620. doi:10.1590/abd1806-4841.20164741
7. Ren H, Zhao F, Zhang Q, Huang X, Wang Z. Autophagy and skin wound healing. *Burns Trauma*. 2022;10:tkac003. doi:10.1093/burnst/tkac003
8. Yang Q, Li S, Zhou Z, et al. Trimetazidine mitigates high glucose-induced retinal endothelial dysfunction by inhibiting PI3K/Akt/mTOR pathway-mediated autophagy. *Bioengineered*. 2022;13(3):7515–7527. doi:10.1080/21655979.2022.2048993
9. Sudhahar V, Okur MN, Bagi Z, et al. Akt2 (protein kinase B beta) stabilizes ATP7A, a copper transporter for extracellular superoxide dismutase, in vascular smooth muscle: novel mechanism to limit endothelial dysfunction in type 2 diabetes mellitus. *Arterioscler Thromb Vasc Biol*. 2018;38(3):529–541. doi:10.1161/ATVBAHA.117.309819
10. Sudhahar V, Okur MN, O'Bryan JP, et al. Caveolin-1 stabilizes ATP7A, a copper transporter for extracellular SOD, in vascular tissue to maintain endothelial function. *Am J Physiol Cell Physiol*. 2020;319(5):C933–C944. doi:10.1152/ajpcell.00151.2020
11. Ashino T, Kohno T, Sudhahar V, Ash D, Ushio-Fukai M, Fukai T. Copper transporter ATP7A interacts with IQGAP1, a Rac1 binding scaffolding protein: role in PDGF-induced VSMC migration and vascular remodeling. *Am J Physiol Cell Physiol*. 2018;315(6):C850–C862. doi:10.1152/ajpcell.00230.2018
12. Mehrabi T, Mesgar AS, Mohammadi Z. Bioactive Glasses: a Promising Therapeutic Ion Release Strategy for Enhancing Wound Healing. *ACS Biomater Sci Eng*. 2020;6(10):5399–5430. doi:10.1021/acsbiomaterials.0c00528
13. Li J, Zhai D, Lv F, et al. Preparation of copper-containing bioactive glass/eggshell membrane nanocomposites for improving angiogenesis, antibacterial activity and wound healing. *Acta Biomater*. 2016;36:254–266. doi:10.1016/j.actbio.2016.03.011
14. Salvo J, Sandoval C. Role of copper nanoparticles in wound healing for chronic wounds: literature review. *Burns Trauma*. 2022;10:tkab047. doi:10.1093/burnst/tkab047
15. Masaldan S, Clatworthy SAS, Gamell C, et al. Copper accumulation in senescent cells: interplay between copper transporters and impaired autophagy. *Redox Biol*. 2018;16:322–331. doi:10.1016/j.redox.2018.03.007
16. Ash D, Sudhahar V, Youn SW, et al. The P-type ATPase transporter ATP7A promotes angiogenesis by limiting autophagic degradation of VEGFR2. *Nat Commun*. 2021;12(1):3091. doi:10.1038/s41467-021-23408-1
17. Xiao J, Zhu Y, Huddleston S, et al. Copper metal-organic framework nanoparticles stabilized with folic acid improve wound healing in diabetes. *ACS Nano*. 2018;12(2):1023–1032. doi:10.1021/acsnano.7b01850
18. Zhang R, Jiang G, Gao Q, et al. Sprayed copper peroxide nanodots for accelerating wound healing in a multidrug-resistant bacteria infected diabetic ulcer. *Nanoscale*. 2021;13(37):15937–15951. doi:10.1039/d1nr04687j
19. Phillips E, Penate-Medina O, Zanzonico PB, et al. Clinical translation of an ultrasmall inorganic optical-PET imaging nanoparticle probe. *Sci Transl Med*. 2014;6(260):260ra149. doi:10.1126/scitranslmed.3009524
20. Peng Y, He D, Ge X, et al. Construction of heparin-based hydrogel incorporated with Cu5.4O ultrasmall nanozymes for wound healing and inflammation inhibition. *Bioact Mater*. 2021;6(10):3109–3124. doi:10.1016/j.bioactmat.2021.02.006
21. Zhou W, Zi L, Cen Y, You C, Tian M. Copper sulfide nanoparticles-incorporated hyaluronic acid injectable hydrogel with enhanced angiogenesis to promote wound healing. *Front Bioeng Biotechnol*. 2020;8:417. doi:10.3389/fbioe.2020.00417
22. Fan L, Ge X, Qian Y, et al. Advances in synthesis and applications of self-healing hydrogels. *Front Bioeng Biotechnol*. 2020;8:654. doi:10.3389/fbioe.2020.00654
23. Liu Y, Hsu SH. Synthesis and biomedical applications of self-healing hydrogels. *Front Chem*. 2018;6:449. doi:10.3389/fchem.2018.00449

24. Quan L, Xin Y, Wu X, Ao Q. Mechanism of self-healing hydrogels and application in tissue engineering. *Polymers*. 2022;14(11):2184. doi:10.3390/polym14112184
25. Shariatinia Z. Carboxymethyl chitosan: properties and biomedical applications. *Int J Biol Macromol*. 2018;120(Pt B):1406–1419. doi:10.1016/j.ijbiomac.2018.09.131
26. Semaming Y, Pannengpetch P, Chattipakorn SC, Chattipakorn N. Pharmacological properties of protocatechuic acid and its potential roles as complementary medicine. *Evid Based Complement Alternat Med*. 2015;2015:593902. doi:10.1155/2015/593902
27. Lee SR, Lee S, Moon E, Park HJ, Park HB, Kim KH. Bioactivity-guided isolation of anti-inflammatory triterpenoids from the sclerotia of Poria cocos using LPS-stimulated Raw264.7 cells. *Bioorg Chem*. 2017;70:94–99. doi:10.1016/j.bioorg.2016.11.012
28. Fang X, Liu Y, Lu J, et al. Protocatechuic aldehyde protects against isoproterenol-induced cardiac hypertrophy via inhibition of the JAK2/STAT3 signaling pathway. *Naunyn Schmiedebergs Arch Pharmacol*. 2018;391(12):1373–1385. doi:10.1007/s00210-018-1556-7
29. Liu Y, Wang X, Pang J, et al. Attenuation of Atherosclerosis by protocatechuic acid via inhibition of M1 and promotion of M2 macrophage polarization. *J Agric Food Chem*. 2019;67(3):807–818. doi:10.1021/acs.jafc.8b05719
30. Huang Y, Liang B, Chen X. Exosomal circular RNA circ_0074673 regulates the proliferation, migration, and angiogenesis of human umbilical vein endothelial cells via the microRNA-1200/MEOX2 axis. *Bioengineered*. 2021;12(1):6782–6792. doi:10.1080/21655979.2021.1967077
31. Blinova E, Pakhomov D, Shimanovsky D, et al. Cerium-containing N-acetyl-6-aminohexanoic acid formulation accelerates wound reparation in diabetic animals. *Biomolecules*. 2021;11(6):834. doi:10.3390/biom11060834
32. Altamimi MA, Hussain A, Alshehri S, Imam SS. Experimental design based optimization and ex vivo permeation of desmopressin acetate loaded elastic liposomes using rat skin. *Pharmaceutics*. 2021;13(7):1047. doi:10.3390/pharmaceutics13071047
33. Huang L, Shi Y, Li M, Wang T, Zhao L. Plasma exosomes loaded pH-responsive carboxymethyl cellulose hydrogel promotes wound repair by activating the vascular endothelial growth factor signaling pathway in type 1 diabetic mice. *J Biomed Nanotechnol*. 2021;17(10):2021–2033. doi:10.1166/jbn.2021.3165
34. Asadpour S, Kargozar S, Moradi L, Ai A, Nosrati H, Ai J. Natural biomacromolecule based composite scaffolds from silk fibroin, gelatin and chitosan toward tissue engineering applications. *Int J Biol Macromol*. 2020;154:1285–1294. doi:10.1016/j.ijbiomac.2019.11.003
35. Chen L, Qin Y, Cheng J, et al. A biocompatible PAA-Cu-MOP hydrogel for wound healing. *RSC Adv*. 2020;10(59):36212–36218. doi:10.1039/c9ra10031h
36. Dardmah F, Farahpour MR. Quercus infectoria gall extract aids wound healing in a streptozocin-induced diabetic mouse model. *J Wound Care*. 2021;30(8):618–625. doi:10.12968/jowc.2021.30.8.618
37. Boroujeni MM, Barzi SM, Zafari M, et al. Electrosprayed cefazolin-loaded niosomes onto electrospun chitosan nanofibrous membrane for wound healing applications. *J Biomed Mater Res B Appl Biomater*. 2022;110(8):1814–1826. doi:10.1002/jbm.b.35039
38. Farahpour MR, Hesaraki S, Faraji D, Zeinalpour R, Aghaei M. Hydroethanolic Allium sativum extract accelerates excision wound healing: evidence for roles of mast-cell infiltration and intracytoplasmic carbohydrate ratio. *Br J Pharmaceutical Sci*. 2017;53(1):e15079. doi:10.1590/s2175-97902017000115079
39. Farahpour MR, Vahid M, Oryan A. Effectiveness of topical application of ostrich oil on the healing of Staphylococcus aureus- and Pseudomonas aeruginosa-infected wounds. *Connect Tissue Res*. 2018;59(3):212–222. doi:10.1080/03008207.2017.1350174
40. Daghian SG, Farahpour MR, Jafarirad S. Biological fabrication and electrostatic attractions of new layered silver/talc nanocomposite using Lawsonia inermis L. and its chitosan-capped inorganic/organic hybrid: investigation on acceleration of Staphylococcus aureus and Pseudomonas aeruginosa infected wound healing. *Mater Sci Eng C Mater Biol Appl*. 2021;128:112294. doi:10.1016/j.msec.2021.112294
41. Choodari Gharehpapagh A, Farahpour MR, Jafarirad S. The biological synthesis of gold/perlite nanocomposite using Urtica dioica extract and its chitosan-capped derivative for healing wounds infected with methicillin-resistant Staphylococcus aureus. *Int J Biol Macromol*. 2021;183:447–456. doi:10.1016/j.ijbiomac.2021.04.150
42. Srivastava P, Kowshik M. Fluorescent lead(IV) sulfide nanoparticles synthesized by Idiomarina sp. strain PR58-8 for bioimaging applications. *Appl Environ Microbiol*. 2017;83(7):e03091–16. doi:10.1128/AEM.03091-16
43. Fan X, Wang X, Cai Y, Xie H, Han S, Hao C. Functionalized cotton charcoal/chitosan biomass-based hydrogel for capturing Pb2+, Cu2+ and MB. *J Hazard Mater*. 2022;423(PtB):127191. doi:10.1016/j.jhazmat.2021.127191
44. Hammud HH, Nemer G, Sawma W, et al. Copper-adenine complex, a compound, with multi-biochemical targets and potential anti-cancer effect. *Chem Biol Interact*. 2008;173(2):84–96. doi:10.1016/j.cbi.2008.03.005
45. Pandit AH, Nisar S, Imtiyaz K, et al. Injectable, Self-Healing, and Biocompatible N, O-Carboxymethyl Chitosan/Multialdehyde Guar Gum Hydrogels for Sustained Anticancer Drug Delivery. *Biomacromolecules*. 2021;22(9):3731–3745. doi:10.1021/acs.biomac.1c00537
46. Ren X, Han Y, Wang J, et al. An aligned porous electrospun fibrous membrane with controlled drug delivery - An efficient strategy to accelerate diabetic wound healing with improved angiogenesis. *Acta Biomater*. 2018;70:140–153. doi:10.1016/j.actbio.2018.02.010
47. Bansode RR, Ahmedna M, Svoboda KR, Losso JN. Coupling in vitro and in vivo paradigm reveals a dose dependent inhibition of angiogenesis followed by initiation of autophagy by C6-ceramide. *Int J Biol Sci*. 2011;7(5):629–644. doi:10.7150/ijbs.7.629
48. Lin YW, Liu PS, Pook KA, Wei LN. Glyburide and retinoic acid synergize to promote wound healing by anti-inflammation and RIP140 degradation. *Sci Rep*. 2018;8(1):834. doi:10.1038/s41598-017-18785-x
49. Nosrati H, Aramideh Khouy R, Nosrati A, et al. Nanocomposite scaffolds for accelerating chronic wound healing by enhancing angiogenesis. *J Nanobiotechnology*. 2021;19(1):1. doi:10.1186/s12951-020-00755-7
50. Jiang T, Li Q, Qiu J, et al. Nanobiotechnology: applications in chronic wound healing. *Int J Nanomedicine*. 2022;17:3125–3145. doi:10.2147/IJN.S372211
51. Urso E, Maffia M. Behind the link between copper and angiogenesis: established mechanisms and an overview on the role of vascular copper transport systems. *J Vasc Res*. 2015;52(3):172–196. doi:10.1159/000438485
52. Zafari M, Boroujeni MM, Omidghaemi S, et al. Physical and biological properties of blend-electrospun polycaprolactone / chitosan-based wound dressings loaded with N-decyl-N, N-dimethyl-1-decanaminium chloride: an in vitro and in vivo study. *J Biomed Mater Res B Appl Biomater*. 2020;108(8):3084–3098. doi:10.1002/jbm.b.34636
53. Mourya VK, Inamdara N, Ashutosh Tiwari N. Carboxymethyl chitosan and its applications. *Adv Materials Lett*. 2010;1(1):11–33. doi:10.1111/j.1365-2273.1996.tb01024